Polymer 51 (2010) 5516–5524

Contents lists available at ScienceDirect

Polymer

journal homepage: www.elsevier.com/locate/polymer

Block copolymer/ionic liquid films: The effect of ionic liquid composition on morphology and ion conduction

Liang Gwee [a,1], Jae-Hong Choi [b,1], Karen I. Winey [b,*], Yossef A. Elabd [a,*]

[a] Department of Chemical and Biological Engineering, Drexel University, Philadelphia, PA 19104, United States
[b] Department of Materials Science and Engineering, University of Pennsylvania, Philadelphia, PA 19104, United States

ARTICLE INFO

Article history:
Received 13 July 2010
Received in revised form
3 September 2010
Accepted 12 September 2010
Available online 18 September 2010

Keywords:
Ionic liquids
Block copolymers
Ionic conductivity

ABSTRACT

The effect of morphology on ion transport in ionic liquid-based solid-state films was investigated. In this study, mixtures of a block copolymer, poly(styrene-*b*-methyl methacrylate) (SbMMA), and an ionic liquid (IL), 1-ethyl-3-methylimidazolium bis (trifluoromethylsulfonyl)imide (EMIm-TFSI), were prepared as clear solid-state films at various IL compositions (0–50 wt%) by solution casting from a volatile co-solvent. The IL was preferentially miscible with the MMA block as evidenced by visual inspection and differential scanning calorimetry. Both equilibrium and non-equilibrium morphologies were identified with X-ray scattering and transmission electron microscopy and the morphology varied with MMA/IL volume fraction. The morphology and microdomain orientation had a significant impact on ionic conductivity. Higher through-plane conductivities were observed in morphologies with a three-dimensionally continuous conducting path (e.g., non-conducting S cylinders) compared to morphologies with a non-continuous conducting path (e.g., lamellae). When the lamellae were oriented in the plane, the through-plane conductivity was significantly lower than the in-plane conductivity, while the conductivity was direction-independent when the morphologies have a continuous conductive path. Also, a significant increase in conductivity was observed with increasing IL content at the glass transition of the conductive (MMA/IL) microdomain. Finally, significantly higher ionic conductivities can be achieved in a block copolymer/IL solid-state film compared to a homopolymer/IL film at the same IL content (wt%), because the non-conductive microdomain excludes IL, which produces a higher local IL concentration in the conductive phase.

© 2010 Elsevier Ltd. All rights reserved.

1. Introduction

The combination of polymers and ionic liquids (ILs) has attracted significant interest, [1] specifically as replacements for current solid-state polyelectrolytes in energy devices, such as dye-sensitized solar cells, [2] supercapacitors, [3] lithium ion batteries, [4] and fuel cells. [5] ILs are organic salts that are liquids at room temperature and have relatively low melting points due to the large size, asymmetry and delocalized charge of the ions. Their resulting unique physiochemical properties (e.g., negligible vapor pressure, high conductivity, wide electrochemical window, high chemical and thermal stability) have motivated, in large part, this investigation into the properties and uses of polymer/IL mixtures. Polymer types that have been explored in these mixtures include homopolymers, [6] copolymers, [7,8] crosslinked polymers, [9] and more recently block copolymers. [10–24] Ionic conductivities as high as 20 mS/cm at 100 °C have been reported in crosslinked ionic gels of poly(methyl methacrylate) (PMMA) and 1-ethyl-3-methylimidazolium bis(trifluoromethylsulfonyl)imide (EMIm-TFSI). [9] A typical result for miscible polymer/IL mixtures is the relationship between conductivity and IL content, where in ionic conductivity is retarded at low IL contents due to the presence of the polymer, while high IL contents produce conductivities approaching that of the bulk ionic liquid. However, increasing IL content also results in plasticization of the polymer (lower mechanical strength) until the mixture progresses from a solid film to a viscous solution with increasing in IL content.

Block copolymers provide a unique opportunity in polymer/IL mixtures, where a variety of nanoscale, self-assembled morphologies can be accessed as a function of composition and thermodynamic incompatibility. Recently, several researchers have investigated the properties of block copolymer/IL mixtures. [10–24] A few studies

* Corresponding authors. Tel.: +1 215 895 0986; fax: +1 215 895 5837.
E-mail addresses: winey@seas.upenn.ed (K.I. Winey), elabd@drexel.edu (Y.A. Elabd).
[1] Equal contributions from both authors.

0032-3861/$ – see front matter © 2010 Elsevier Ltd. All rights reserved.
doi:10.1016/j.polymer.2010.09.026

have characterized both the lyotropic and thermotropic phase behavior for several block copolymer/IL mixtures over a broad IL composition range. [16,20] However, most investigations on block copolymer/IL mixtures have focused on the high IL composition range identifying unique solution and gel behavior. At high IL contents, all micellar structures have been identified in several different block copolymer/IL systems similar to what has been observed in amphiphilic block copolymer/water solutions, but with different thermosensitivity. [10,11,14] Lodge and coworkers [12,15,19] have utilized this behavior in their demonstration of thermoreversible transfer of block copolymer micelles between water and IL; this is a unique pathway where a block copolymer can be used as a carrier of small molecules from one media to the next. To date, only several publications have reported on the ionic conductivity of block copolymer/IL mixtures, which is a property of great interest as it relates to the performance of energy devices. He et al. [13] reported on the conductivity of the triblock copolymer poly(styrene-*b*-ethylene oxide-*b*-styrene) in the IL 1-butyl-3-methylimidazolium hexafluorophosphate (BMIm-PF_6) at the high IL composition range (>90 wt%). In this concentration range, the block copolymer appears to not have a significant impact on the IL conductivity, where the conductivity decreases with increasing viscosity similar to neat ILs. More recently, Simone and Lodge [24] report on the ionic conductivity of mixtures of the diblock poly (styrene-*b*-ethylene oxide) and EMIm-TFSI in the concentrated solution regime, where conductivity increased with increasing IL concentration and molecular weight of the ethylene oxide block. With only a few reports on the conductivity of block copolymer/IL mixtures, questions still remain regarding the mechanisms of ion transport and the ability to attain high conductivities in mechanically robust solid-state films.

In this study, we focus on the solid-state properties of block copolymer/IL mixtures and their potential impact to solid-state energy devices. Specifically, we study the morphology and ion conductivity of free standing films of an IL, 1-ethyl-3-methylimidazolium bis (triflouromethylsulfonyl)imide (EMIm-TFSI), and a diblock copolymer, poly(styrene-*b*-methyl methacrylate) (SbMMA). This study illustrates the significant impact both morphology and microdomain orientation can have on ionic conductivity and also the benefits of the block copolymer/IL mixtures, where significantly higher ionic conductivities can be achieved in this system compared to its homopolymer/IL counterpart.

2. Experimental

2.1. Materials

1-ethyl-3-methylimidazolium bis (trifluoromethylsulfonyl) imide (EMIm-TFSI) (mol. wt. = 394.36 g/mol; 99% purity) was purchased from Io-li-tec and used as received. Poly(methyl-methacrylate) (PMMA) and poly(styrene) (PS) were both purchased from Scientific Polymer Products with the reported molecular weights of 75,000 g/mol and 210,000 g/mol, respectively. PS was used as received, while PMMA was placed in a vacuum oven for 2 days at 110 °C prior to use. Diblock copolymer, poly (stryrene-*b*-methyl methacrylate) (SbMMA) (Mn (S) = 33,000 g/mol; Mn (SbMMA) = 39,000 g/mol; PDI (S) = 1.06; PDI (SbMMA) = 1.09) was purchased from Polymer Source and used as received. A mass fraction of 0.555 of MMA in the block copolymer was calculated using integrated ^{1}H NMR signals of the neat block copolymer. N-N-dimethylacetamide (DMAc) (99.8%) and toluene (99.5%) were both purchased from Aldrich and were used as received.

2.2. Film preparation

Each polymer was dissolved in DMAc or toluene at 5% (w/v). After stirring for ~12 h, a specified amount of EMIm-TFSI was added to the solutions and allowed to stir for an additional ~2 h to form a homogeneous, clear solution. The polymer-ionic liquid mixture was then cast into a Teflon Petri dish under nitrogen atmosphere for ~2 days. This casting procedure occurred at 50 °C for solutions with DMAc and at room temperature for solutions with toluene. Resulting films were annealed with one of two annealing procedures: ~2 days at 110 °C under vacuum followed by a natural cooling to room temperature or ~7 days at 110 °C under vacuum followed by a rapid quench in liquid nitrogen. After annealing, all films (thicknesses in the range of 200–300 μm) were stored in a desiccator to minimize any uptake of atmospheric moisture and extreme care was taken to ensure that samples were not exposed to the environment prior to each experiment.

2.3. Differential scanning calorimetry

Thermal transitions were measured using TA Q2000 differential scanning calorimeter (DSC). Stacked samples weighing ~5–10 mg

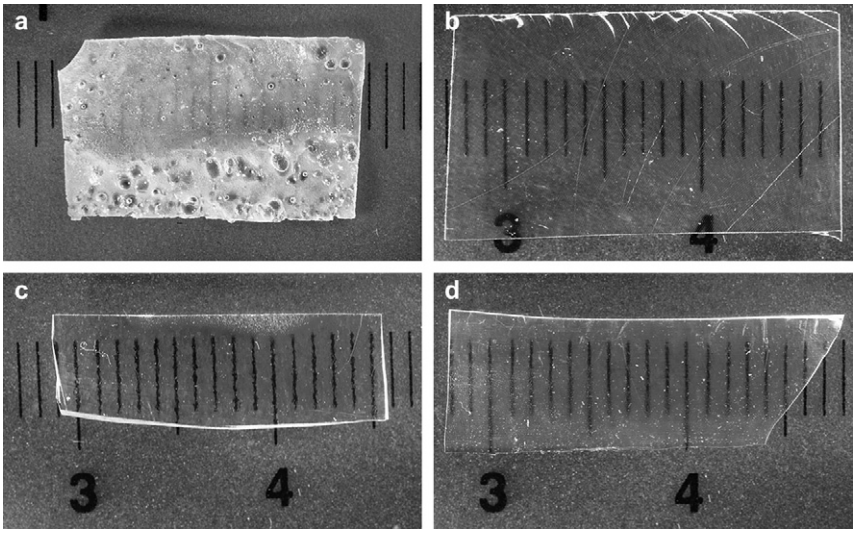

Fig. 1. Optical images of polymers with 40 wt% IL where the polymers are (a) PS, (b) PMMA, and (c, d) SbMMA. (a), (b), and (c) were solution cast from DMAc and annealed for 2 days at 110 °C; (d) was solution cast from toluene and annealed for 7 days at 110 °C.

were sealed in Tzero aluminum pans and heated to 150 °C at 10 °C/min, held at 150 °C for 1 min, cooled to 110 °C rapidly, held at 110 °C for 10 min, cooled to −150 °C rapidly, held at −150 °C for 10 min, and then heated again to 150 °C at 10 °C/min under a nitrogen atmosphere. Glass transition temperatures were measured from the second heating cycle using the mid-point method.

2.4. Morphology

X-ray scattering was performed on the films along two directions (through-plane and in-plane) with a small angle X-ray scattering (SAXS) system, which generates Cu X-ray from a Nonius FR 591 rotating-anode generator operated at 40 kV and 85 mA. The bright, highly collimated beam was obtained via Osmic Max-Flux optics and pinhole collimation in an integral vacuum system. The scattering data were collected using a Brukers Hi Star two-dimensional detector with a sample to detector distance of 150 cm. Using Datasqueeze software, [25] azimuthal angle (0–360°) integration was used to convert 2-D through-plane patterns to 1-D data, intensity was corrected for primary beam intensity, and the corrected scattering from an empty cell was subtracted. The lattice types and lattice parameters of the samples were determined from X-ray scattering data. All the observed peaks were included in calculating the lattice parameter by a linear regression method using the experimental interplanar spacings and the assigned Miller indices. [26,27] Morphology was also imaged using a JEM 1400 transmission electron microscope (TEM) operating at 120 kV, where images were recorded on an ORIUS™ TEM CCD camera. Each sample was sectioned at room temperature using a Reichert–Jung ultramicrotome with a diamond knife to a nominal thickness of 30–50 nm. The contrast between the PS and PMMA domains was enhanced by RuO_4 staining.

2.5. Ionic conductivity

The ionic conductivity of each film was measured both through-plane and in-plane with electrochemical impedance spectroscopy (EIS), where the conductors are the anions and cations of the IL. Film resistance was measured at 10 mV over a range of AC frequencies (100 Hz–1 MHz) using a Solartron impedance system (1260 impedance analyzer, 1287 electrochemical interface, Zplot software). Through-plane conductivity was measured using a two-electrode cell, which consisted of sandwiching each film between two stainless steel polished blocking electrodes (surface area = 1.2161 ± 0.0015 cm^2) within a sealable Telfon custom-made cell. In-plane conductivity was measured using a four-electrode configuration, where resistance was measured between two inner reference electrodes (~3 mm apart) and potential applied to the outer electrodes (~3 cm apart) on the surface of the film. A schematic diagram of both the two and four-electrode apparatus are provided elsewhere. [28] Each film was sealed in a custom-made four-electrode cell with the adequate pressure applied between electrodes and film. The cell has openings to expose the film to a controlled environment. The four-electrode cell was placed in a Tenney chamber with electrical feedthroughs, where resistance was measured as a function of temperature at a fixed relative humidity (10% RH). In-plane experiments were collected using the same impedance system and frequency ranges as reported for the through-plane experiments.

For both through-plane and in-plane experiments, the real impedance (resistance) was determined from the *x*-intercept of the imaginary versus real impedance data (Nyquist plot) over a high frequency range. Film conductivity for through-plane experiments were calculated using the real impedance, film thickness, and electrode area, while in-plane conductivity was calculated using

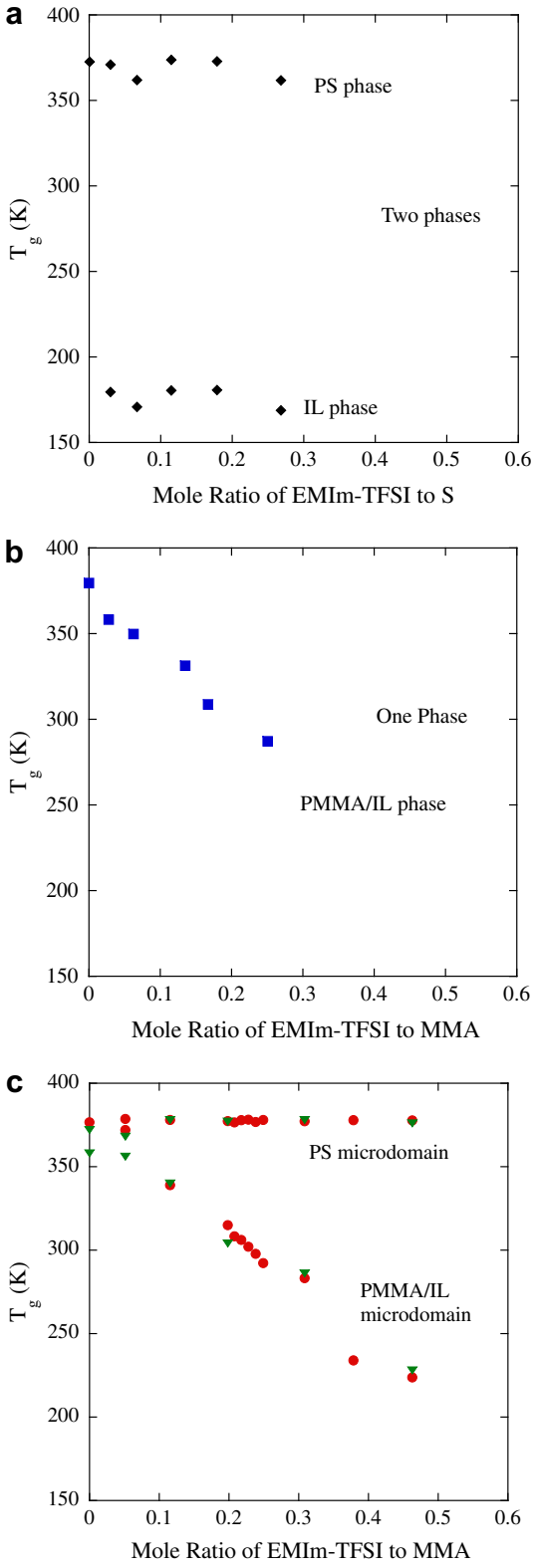

Fig. 2. Glass transition temperatures of (a) PS/IL (◆), (b) PMMA/IL (■), and (c) SbMMA/IL – cast from DMAc and annealed for 2 days at 110 °C (▼) and cast from toluene and annealed for 7 days at 110 °C (●). (a) and (b) were cast from DMAc and annealed for 2 days at 110 °C.

the real impedance, distance between electrodes (~3 mm), and the cross-sectional area for conduction (membrane width times thickness). The film thickness of each sample was measured with a micrometer (Mitutoyo) with 1 μm accuracy. Conductivity values for each sample reported for the through-plane experiments are an average of at least three experiments conducted on three separate specimens. More details regarding the procedures have documented elsewhere. [28]

3. Results and discussion

3.1. Morphology of SbMMA/IL mixtures

Optical images of several solution-cast polymer/IL mixture films are shown in Fig. 1. Both the homopolymer PMMA (Fig. 1b) and block copolymer SbMMA (Fig. 1c and d) produced transparent films when cast with IL, while the hompolymer PS (Fig. 1a) produced an opaque film. These results indicate that the IL EMIm-TFSI is preferentially compatible with PMMA over PS.

Fig. 2 shows the glass transition temperatures of the polymer/IL films measured by DSC. Although samples were prepared on a mass basis, all of the graphs in Fig. 2 were plotted on a mole ratio basis to allow for a direct comparison of the MMA phase in both homopolymer and block copolymer films. DSC results on the pure IL, EMIm-TFSI, showed three different thermal transitions: glass transition at 180 K, crystallization at 215 K, and melting at 254 K. These results compare well with Noda et al. [29] For the PS/IL system, all of these transitions were observed in addition to the glass transition of PS (~373 K). Fig. 2a shows the measured glass transition temperatures for the IL and PS in the PS/IL films, where there is no significant change in either glass transition with increasing IL content. In contrast, the PMMA/IL system exhibits one glass transition at all IL contents, Fig. 2b, and decreases with increasing IL. A noticeable plasticization effect was observed, where transparent PMMA films were brittle and became increasingly more flexible at higher IL contents. Fig. 2c shows two measured glass transitions for the block copolymer/IL films for both casting solvents used. Similar to the PMMA/IL films, there is a single T_g for the MMA/IL microdomain, which decreases with increasing IL content, while there is also a single T_g for the S, which does not change with increasing IL content. The two measured glass transitions of the pure SbMMA confirm block copolymer microphase separation, as expected. Two glass transition temperatures persist at all IL contents and the T_g for the MMA/IL microdomain decreases. Note that the glass transition temperatures of the MMA phase in both the homopolymer (Fig. 2b) and block copolymer (Fig. 2c) are comparable at all IL to MMA mole ratios. These results, in conjunction with the physical appearance of the films (Fig. 1), demonstrate that the IL preferentially segregates to the MMA block in the block copolymer.

Fig. 3 shows the X-ray scattering results for SbMMA/IL films solution cast from toluene. The through-plane and in-plane 2-D scattering patterns for the pure SbMMA film (Fig. 3a) reveal a macroscopic isotropic morphology. In contrast, the 2-D scattering patterns for the SbMMA/IL with 30 wt% IL (Fig. 3b) shows anisotropic morphology with domains preferentially oriented in the plane of the film. SbMMA/IL films at all other IL contents also show a similar anisotropic morphology. The 2-D through-plane patterns were integrated to give the 1-D scattering patterns in Fig. 3c. The SbMMA films show lamellar morphologies at 0–34 wt% IL and cylindrical morphologies at 35–50 wt% IL; see also Table 1. Under equilibrium conditions, a lamellar morphology was expected for the pure SbMMA film with this volume fraction of MMA (0.52), as well as the transition to S cylinders in an MMA/IL matrix with increasing MMA/IL volume fraction; volume fractions given in Table 1.

Fig. 4 shows the X-ray scattering results for SbMMA/IL films that were solution cast from DMAc. The 2-D scattering patterns in Fig. 4a and b reveal similar results as was observed in Fig. 3a and b; isotropic morphology for SbMMA and anisotropic morphology for SbMMA/IL at all IL contents. Again, the through-plane 2-D patterns

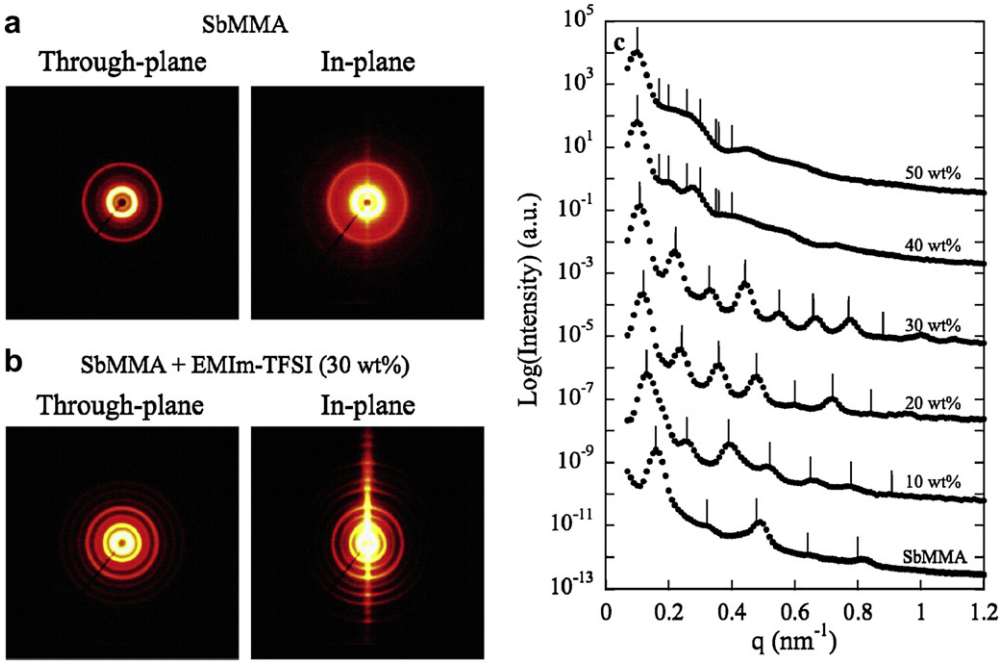

Fig. 3. X-ray scattering of SbMMA/IL films solution cast from toluene and annealed for 7 days at 110 °C. Through-plane and in-plane 2-D small angle X-ray scattering patterns of SbMMA at (a) 0 and (b) 30 wt% IL. (c) Through-plane 1-D X-ray scattering intensity versus scattering vector as a function of IL content. Expected peak positions for lamellar (0, 10, 20, 30 wt%) and cylindrical (40, 50 wt%) morphologies are shown. The excess scattering in the vertical direction in the 2-D in-plane scattering arises from the surface reflection, because the X-ray beam is wider than the film thickness.

Table 1
Morphology of SbMMA/IL films.

IL Content (wt%)	IL to MMA (mole ratio)	Volume fraction ϕ_c(MMA + IL)[a]	Toluene		DMAc	
			Morphology	Lattice Parameter (nm)[b]	Morphology	Lattice Parameter (nm)[b]
0	0.00	0.519	Lamellar	39	Microphase Separated	33[c]
10	0.051	0.555	Lamellar	48	Microphase Separated	37[c]
20	0.115	0.594	Lamellar	52	Cylinder	48
30	0.198	0.635	Lamellar	57	Cylinder	56
31	0.208	0.639	Lamellar	60	–	–
32	0.218	0.643	Lamellar	60	–	–
33	0.228	0.647	Lamellar	59	Microphase Separated	36[c]
34	0.238	0.652	Lamellar	59	–	–
35	0.249	0.656	Cylinder	72	–	–
37	0.272	0.665	–	–	Microphase Separated	37[c]
40	0.309	0.678	Cylinder	73	Microphase Separated	42[c]
50	0.463	0.724	Cylinder	73	Microphase Separated	42[c]

[a] Volume fraction (ϕ_c) of IL swollen MMA phase was calculated based on the densities of PS (1.04), PMMA (1.2) and IL (1.52) assuming no volume change upon mixing.
[b] Lattice parameter obtained through SAXS analysis calculated based on a linear regression method using the experimental interplanar spacings and the assigned Miller indices. [26,27].
[c] Correlation distance calculated based on $d = 2\pi/q_1$, where the q_1 is the primary peak position in the 1-D SAXS plot.

were integrated to give the 1-D scattering patterns in Fig. 4c. However, unlike the toluene-cast and annealed (7 days, 110 °C) samples, the morphologies of the DMAc-cast and annealed (2 days, 110 °C) samples are generally insufficiently ordered to permit identification of the morphology type. The dash markings in Fig. 4c for the 20 and 30 wt% IL samples correspond to cylinders on a hexagonal lattice, where the calculated form factor scattering for these samples weakens the second order reflections. Thus, the 20 and 30 wt% IL films appear to have hexagonal symmetry. [30] In an attempt to transform the morphologies in the DMAc-cast samples to those of the toluene-cast samples, the annealing time was increased to 7 days at 110 °C and a liquid nitrogen quench was introduced, but the poorly-ordered morphologies persisted. The differences in morphologies between the toluene and DMAc-cast samples can be explained by differences in solvent and block solubility parameters, namely toluene is selective for PS, while DMAc (and EMIm-TFSI) is selective for PMMA. [31,32]

The morphology assignments from X-ray scattering data were confirmed with TEM. Fig. 5 shows TEM images of representative samples. The TEM image of the pure SbMMA film cast from DMAc (Fig. 5c) shows a microphase-separated morphology, but randomly distributed microdomains, which are indicative of a non-equilibrium state. In contrast, the pure SbMMA film cast from toluene (Fig. 5d) shows the expected lamellar morphology. Hexagonally packed cylinders of S in MMA/IL can be observed for the SbMMA/IL (20 wt%) film cast from DMAc (Fig. 5a), while a lamellae morphology for the same IL composition was observed when cast from toluene (Fig. 5b).

3.2. Conductivity of SbMMA/IL mixtures

Fig. 6 shows the through-plane room temperature ionic conductivity of PMMA/IL and toluene-cast SbMMA/IL films as a function of IL composition relative to MMA, which facilitates

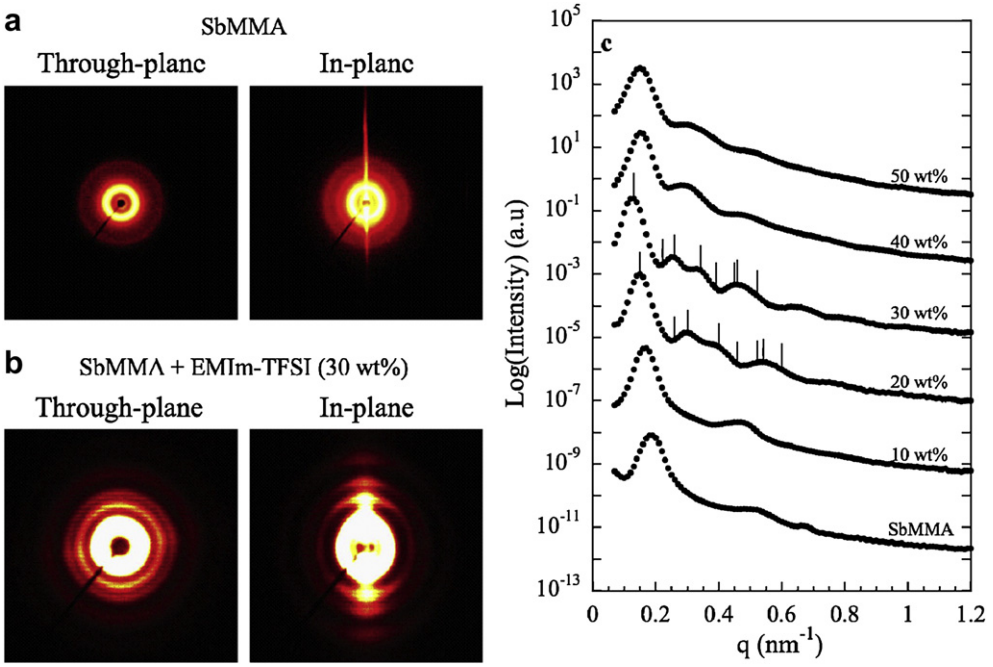

Fig. 4. X-ray scattering of SbMMA/IL films solution cast from DMAc and annealed for 2 days at 110 °C. Through-plane and in-plane 2-D small angle X-ray scattering patterns of SbMMA at (a) 0 and (b) 30 wt% IL. (c) Through-plane 1-D X-ray scattering intensity versus scattering vector as a function of IL content. Expected peak positions for cylindrical morphologies are shown.

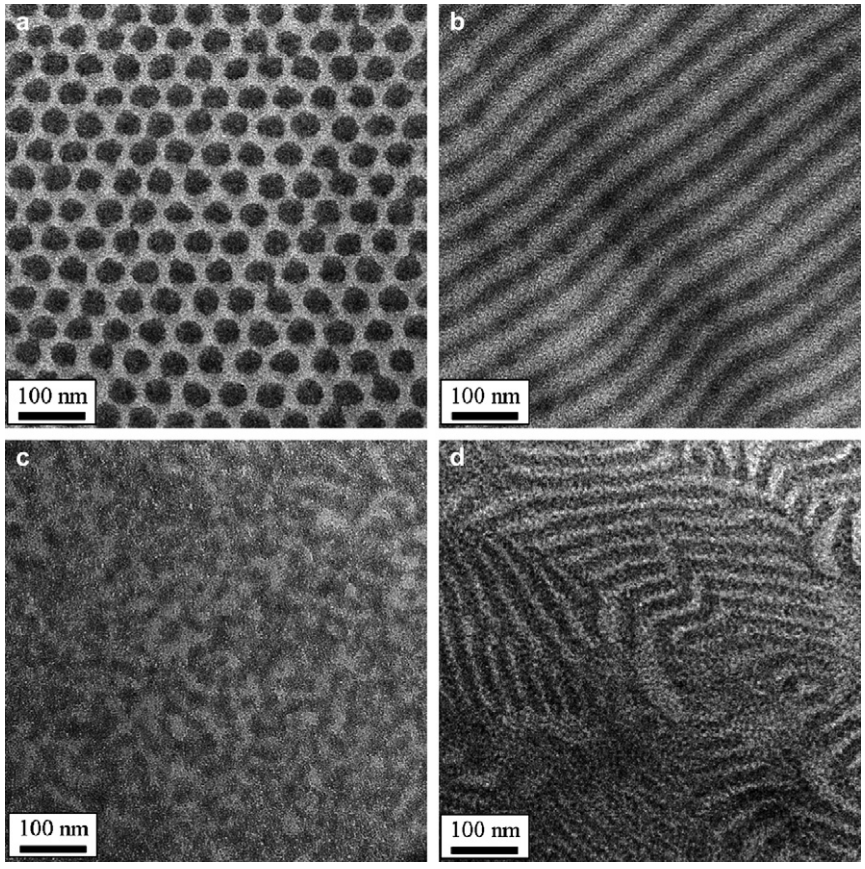

Fig. 5. Transmission electron microscopy images of SbMMA/IL (20 wt%) (a, b) and SbMMA (c, d) films. (a, c) were solution cast from DMAc and annealed for 2 days at 110 °C and stained by RuO_4. (b, d) were solution cast from toluene and annealed for 7 days at 110 °C and were not stained. The dark regions correspond to the S microdomains in (a,c), while the MMA/IL microdomains appear dark in (b,d) due to electron density differences.

a comparison between the homopolymer/IL and block copolymer/IL films. A sharp increase in conductivity was observed in the mixtures containing both the homopolymer (at ~0.15 mol ratio) and the block copolymer (at ~0.2 mol ratio). These IL compositions approximately correspond to the IL composition at which T_g is room temperature (see Fig. 2), which is the temperature of the conductivity experiments. In other words, the transition from a glassy to a rubbery state in the polymer results in a significant increase in conductivity for both systems due to the increased segmental motion of the PMMA chains and increased free volume.

Additionally, clear differences in conductivity can be observed when comparing the homopolymer to the block copolymer at each IL composition. The homopolymer exhibits higher conductivities compared to the block copolymer at similar IL mole ratios and glass transition temperatures. Interestingly, at 50 wt%, the conductivity is substantially higher for the SbMMA/IL (~0.45 mol ratio; $\sim 2 \times 10^{-5}$ S/cm) than for the PMMA/IL (~0.25 mol ratio; $\sim 4 \times 10^{-6}$ S/cm). When PMMA/IL mixtures at higher IL content were prepared, the result was a viscous solution and free-standing solid-state films were not attainable. In contrast, the SbMMA allows for the preparation of solid-state films at higher IL to MMA mole ratios, because the PS microdomain (the non-conducting block) retains its high glass transition temperature and imparts improved mechanical stability. Thus, block copolymer/IL films can access higher ionic conductivities than the homopolymer/IL films by reaching higher IL to MMA ratios.

Fig. 7 shows the measured through-plane conductivity for the SbMMA/IL samples cast from both toluene and DMAc as a function of the volume fraction of the conductive microdomain of the block copolymer films to examine the importance of block copolymer morphology. This data was compared to the maximum predicted conductivity calculated from a parallel model assuming perfect long-range order of alternating conductive and non-conductive

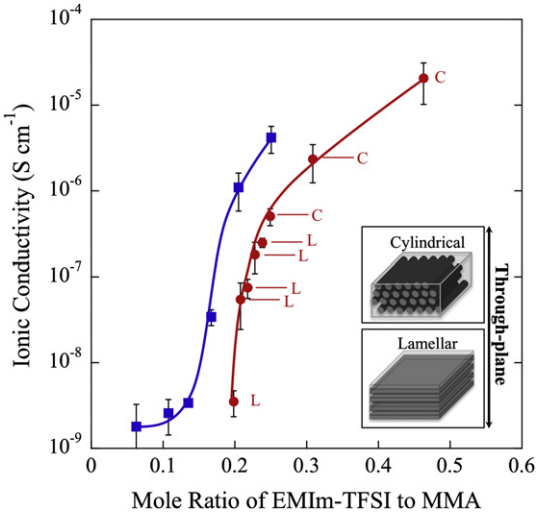

Fig. 6. Through-plane ionic conductivity of PMMA/IL (■) and toluene-cast SbMMA/IL (●) films at room temperature as a function of IL to MMA mole ratio. The schematics show the two idealized block copolymer morphologies and the direction of measured ion transport. The labels (C, L) represent cylindrical, and lamellar morphologies, respectively. The trend lines help to guide the eye.

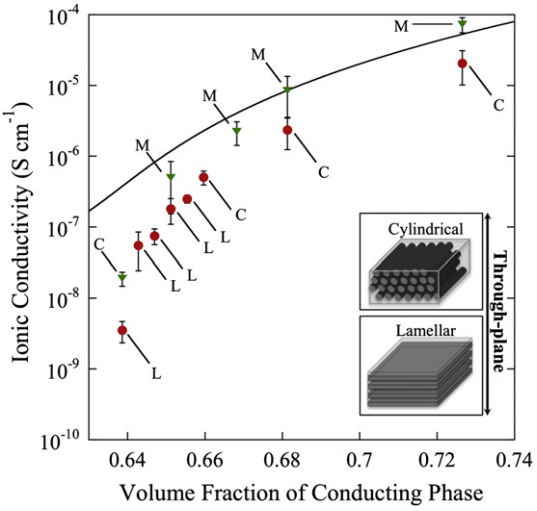

Fig. 7. Room temperature through-plane conductivity of toluene-cast (●) and DMAc-cast (▼) SbMMA/IL films compared with the maximum predicted conductivity (σ_{max} – solid line) for perfect lamellae aligned in the direction of ion transport. The schematics illustrate the two idealized block copolymer morphologies and the direction of measured ion transport.

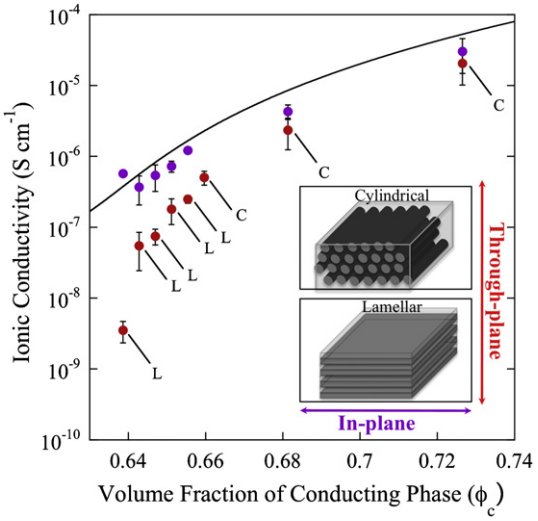

Fig. 8. Room temperature through-plane (●) and in-plane (●) ionic conductivity of toluene-cast SbMMA/IL films compared with maximum predicted conductivity (σ_{max} – solid line) for perfect lamellae aligned in the direction of transport. The schematics illustrate the two idealized block copolymer morphologies and the directions of measured ion transport.

lamellar domains where the normal of the lamellae is perpendicular to the measured direction of transport (shown in Eq. (1)):

$$\sigma_{max} = \phi_c\sigma_c + (1-\phi_c)\sigma_n \quad (1)$$

In Eq. (1), ϕ_c is the volume fraction of the conductive microdomain (MMA + IL) and σ_c and σ_n are the conductivities of the conductive and non-conductive microdomains, respectively. If we assume that the $\sigma_n = 0$, then Eq. (1) simplifies to: [33]

$$\sigma_{max} = \phi_c\sigma_c \quad (2)$$

where σ_c is the composition-dependent conductivity measured for the homopolymer PMMA/IL films (data in Fig. 6).

Fig. 7 compares the idealized σ_{max} with the experimental through-plane conductivity of the block copolymer/IL films. When the conductive microdomains are glassy ($\phi_c < 0.64$), the anisotropic lamellar morphology results in significantly lower through-plane conductivities than the predicted maximum value. (Note that the lamellar domains are preferentially oriented in the plane of the film, which is opposite the direction of transport; see inset in Fig. 7.) The films with a cylindrical morphology, where the conductive microdomain has continuity in three dimensions throughout the film and the discrete cylinders are the non-conducting styrene, results in conductivities closer to σ_{max}, while the films with microphase-separated morphologies results in even higher conductivities. The conductivity differences between lamellar and cylindrical morphologies illustrate the differences between preferentially oriented conductive domains opposite the direction of transport to a more continuous path for transport. The differences between periodic cylindrical and non-periodic microphase-separated morphologies may be the result of differences in grain boundaries or macroscopic connectivity of MMA/IL microdomains.

The effect of morphology on ionic conductivity can be more clearly seen in Fig. 8, which shows both the through-plane and in-plane conductivities of the toluene-cast SbMMA/IL films; see figure inset. There is a significant difference between the through-plane and in-plane conductivity for the films with an anisotropic lamellar morphology. In these results, the effect of anisotropic lamellar morphology on conductivity can be clearly observed both when the conductive phase is glassy ($\phi_c < 0.64$) and rubbery ($\phi_c = 0.64$–0.67). As expected, the measured conductivity is in better agreement with σ_{max} when the lamellar microdomains are along the measurement direction.

At higher IL compositions ($\phi_c > 0.68$), where the cylindrical morphology is observed, the difference in conductivity between the two orthogonal measurement directions is statistically insignificant. Although the non-conductive cylinders are in a preferential anisotropic orientation, the conductive MMA/IL microdomain is continuous throughout the film. These results demonstrate the significant effect that orientation of morphology can have on ion transport. Additionally, the SbMMA/IL films cast from DMAc that exhibit a continuous conductive microdomain within cylinderical and microphase-separated morphologies also result in comparable through-plane and in-plane conductivities. Finally, it is important to note the several measured conductivities are greater than σ_{max} as shown in Figs. 7 and 8. In Eq. (2), σ_{max} is calculated from σ_c, the measured conductivity of homopolymer PMMA/IL mixture. These results suggest that the conductivity in the MMA/IL microdomain is higher than the PMMA/IL mixture at a fixed MMA:IL ratio, which implies the presence of a local IL concentration gradient within the conducting microdomains that facilitates ion transport.

Fig. 9 shows regressions of the toluene-cast SbMMA/IL films conductivity-temperature data to the Vogel–Tamman–Fulcher (VTF) equation, $\sigma = \sigma_0 \cdot \exp[-B/(T-T_0)]$, where σ_0 is the maximum predicted conductivity at infinite temperature, B is related to the Arrhenius activation energy, and T_0 is the Vogel temperature. The VTF equation accounts for the effect of polymer relaxation or segmental motion of polymer chains and is often used to describe ion transport in polymer electrolytes. [34] The data regresses well to the VTF equation (Fig. 9a) and can alternatively be regressed to the same equation with a discontinuity at ~100 °C (Fig. 9b). Coincidentally this temperature corresponds to the glass transition temperature of the S microdomain of the block copolymer. The discontinuous regression is not necessary, but it is interesting to note that there is a slight increase in conductivity after this discontinuity only for the 30 wt% IL sample; this is the only sample with a lamellar morphology in Fig. 9. The Vogel temperatures determined from both the continuous (Fig. 9a) and discontinous (Fig. 9b) VTF regressions are shown in Table 2. The Vogel

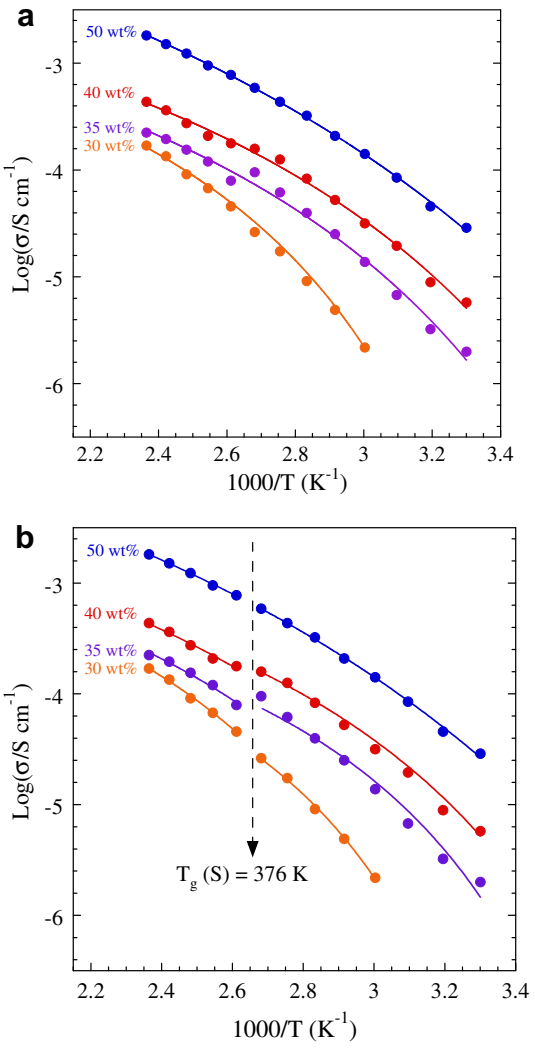

Fig. 9. Temperature dependence of in-plane ionic conductivity for toluene-cast SbMMA/IL films. Solid lines represent regression to VTF equation (a) with and (b) without a discontinuity at the non-conductive (S) microdomain glass transition temperature.

temperature may be considered the temperature at which ion conduction ceases and is commonly 50 K below the measured T_g for many polymer electrolytes. [34] In Table 2, the difference between the glass transition and Vogel temperatures match the expected 50 K more closely for the discontinuous regression compared to the continuous regession.

Table 2
Measured glass transition temperatures and Vogel temperatures for SbMMA/IL films.

EMIm-TFSI (wt %)	T_g (K)	$T_g - T_0$ (K) continuous[a]	$T_g - T_0$ (K) discontinuous[b]
30	315	63	53
35	292	80	53
40	283	78	62
50	224	53	51

[a] VTF regression of Fig. 9a.
[b] VFT regression of Fig. 9b for the data below the glass transition of the S microdomain.

4. Conclusions

This work demonstrates that significantly higher ionic conductivities (up to 1 mS/cm at ~100 °C) can be achieved in block copolymer/IL solid-state films compared to its homopolymer counterpart at the same ionic liquid content (wt%). The non-conductive microdomain (S) in the block copolymer is immiscible with the IL and thus retains its high glass transition temperature with increasing IL content and allows for higher IL contents relative to the conductive microdomain (MMA) compared to the homopolymer (PMMA). This work also demonstrates the significant effect that glass transition, morphology, and microdomain orientation have on ionic conductivity in block copolymer/IL solid-state films. The glass transition of the conductive microdomain impacts transport, where a significant increase in conductivity is observed at this transition. Changing morphology from a discontinuous conductive microdomain (anisotropic lamellae morphology) to a continuous conductive microdomain (anisotropic non-conducting cylinders or microphase-separated morphologies) results in increased through-plane conductivities. Also, a significant difference in conductivity was observed when comparing through-plane and in-plane conductivity only for the films with an anisotropic lamellar morphology. Overall, the block copolymer/IL system appears to be highly tunable, where numerous chemistries and morphologies can be envisioned, which can impact solid-state properties and ionic conductivities. Electrochemical devices that require solid-state polymer electrolytes will benefit from the continued development of block copolymer/IL films.

Acknowledgments

This work is supported in part by the U.S. Army Research Office under grant no. W911NF-07-1-0452 Ionic Liquids in Electro-Active Devices (ILEAD) MURI. We thank Louis Madsen and Kyle Wilmsmeyer of Virginia Tech for their NMR characterization of the block copolymer. We thank Chris Murray of the University of Pennsylvania for use of the JEM 1400.

References

[1] Ueki T, Watanabe M. Macromolecules 2008;41:3739.
[2] Kawano R, Matsui H, Matsuyama C, Sato A, Susan MABH, Tanabe N, et al. J Photochem Photobiol A 2004;164:87.
[3] Lee J, Panzer MJ, He Y, Lodge TP, Frisbie CD. Macromolecules 2007;129:4532.
[4] Shin JH, Henderson WA, Scaccia S, Prosini PP, Passerini S. J Power Sources 2006;156:560.
[5] Noda A, Bin Hasan Susan A, Kudo K, Mitsushima S, Hayamizu K, Watanabe M. J Phys Chem B 2003;107:4024.
[6] Martinelli A, Matic A, Jacobsson P, Borjesson L, Navarra MA, Panero S, Scrosati B. J Electrochem Soc 2007;154:G183.
[7] Sekhon SS, Park J-S, Cho E, Yoon Y-G, Kim C-S, Lee W-Y. Macromolecules 2009;42:2054.
[8] Martinelli A, Matic A, Jacobsson P, Borjesson L, Fernicola A, Panero S, et al. J Phys Chem B 2007;111:12462.
[9] Susan M, Kaneko T, Noda A, Watanabe M. J Am Chem Soc 2005;127:4976.
[10] Wang L, Chen X, Chai Y, Hao J, Sui Z, Zhuang W, et al. Chem Commun 2004;24:2840.
[11] He Y, Li Z, Simone P, Lodge TP. J Am Chem Soc 2006;128:2745.
[12] He Y, Lodge TP. J Am Chem Soc 2006;128:12666.
[13] He YY, Boswell PG, Bühlmann P, Lodge TP. J Phys Chem B 2007;111:4645.
[14] Simone PM, Lodge TP. Macromol Chem Phys 2007;208:339.
[15] Bai Z, He Y, Lodge TP. Langmuir 2008;24:5284.
[16] Simone PM, Lodge TP. Macromolecules 2008;41:1753.
[17] Noro A, Matsushita Y, Lodge TP. Macromolecules 2008;41:5839.
[18] Guerrero-Sanchez C, Goh J-F, D'Haese C, Thijs H, Hoogenboom R, Schubert US. Chem Commun 2008;24:2753.
[19] Bai Z, Lodge TP. J Phys Chem B 2009;113:14151.
[20] Virgili JM, Hexemer A, Pople JA, Balsara NP, Segalman RA. Macromolecules 2009;42:4604.
[21] Meli L, Lodge TP. Macromolecules 2009;42:580.
[22] Tamura S, Ueki T, Ueno K, Kodama K, Watanabe M. Macromolecules 2009;42:6239.

[23] Noro A, Matsushita Y, Lodge TP. Macromolecules 2009;42:5802.
[24] Simone PM, Lodge TP. ACS Appl Mater Interfaces 2009;12:2812.
[25] Heiney PA. Comm Powder Diffr Newsletter 2005;32:9.
[26] Winey KI, Thomas EL, Fetters LJ. Macromolecules 1991;24:6182.
[27] Winey KI. PhD Dissertation Thesis. University of Massachusetts, Amherst; 1991.
[28] Elabd YA, Beyer FL, Walker CW. J Membr Sci 2004;231:181.
[29] Noda A, Hayamizu K, Wantanabe M. J Phys Chem B 2001;105:4603.
[30] Richards RW, Thomson JL. Macromolecules 1983;16:982.
[31] Brandrup J, Immergut EH, Grulke EA, Eric A, Akihiro A, Bloch DR. Polymer handbook. 4th ed. New York: John Wiley & Sons; 1999.
[32] Camper D, Becker C, Koval C, Noble R. Ind Eng Chem Res 2005;44:1928.
[33] Robeson LM, Hwu HH, McGrath JE. J Membr Sci 2007;302:70.
[34] Chen H, Choi J-H, Salas-de la Cruz D, Winey KI, Elabd YA. Macromolecules 2009;42:4809.